MAVEN/IUVS Nadir Observations of Discrete Aurora on Mars: Insights into Regional Local Time Control and Magnetic Reconnection

BENJAMIN JACOB JOHNSTON
Department of Astrophysical and Planetary Sciences
Laboratory for Atmospheric and Space Physics
University of Colorado Boulder

Honors Thesis Committee

DR. NICHOLAS SCHNEIDER, Thesis Advisor
Department of Astrophysical and Planetary Sciences
Laboratory for Atmospheric and Space Physics

DR. ANN-MARIE MADIGAN, Honors Council Representative
Department of Astrophysical and Planetary Sciences
Joint Institute for Laboratory Astrophysics

DR. NOAH FINKELSTEIN, Thesis Committee Member
Department of Physics

DR. DAVID BRAIN, Thesis Committee Member
Department of Astrophysical and Planetary Sciences
Laboratory for Atmospheric and Space Physics

Defended 6 April 2022

Abstract

Discrete aurora are sporadic ultraviolet emissions on Mars. These emissions, which occur globally and in the upper atmosphere of Mars, are strongly correlated with martian crustal magnetic field. Crustal fields on Mars form from remanent magnetism locked in the crust, and vary in strength across the disk, with the strongest fields located in the southern hemisphere. Previous studies using data taken by the MAVEN spacecraft has revealed hundreds of detections in limb viewing and a single detection in the nadir observations. Further analysis of all nightside MUV nadir-viewing observations taken by the MAVEN Imaging Ultraviolet Spectrograph (IUVS) instrument has revealed approximately two hundred additional discrete aurora detections. While aurora occur globally and sporadically, events in the strongest crustal magnetic field regions of the martian southern hemisphere show high repeatability. Previous work reported using IUVS limb observations (Schneider et al., 2021) revealed detections occurring before midnight; the emissions identified in the nadir dataset show detections both occurring before midnight and after midnight in the strong field region. We find a previously unreported correlation and between local time and geographic location, with two distinct auroral event groups manifesting pre- and post-midnight in separate but adjacent locations in the strong field region. Magnetic field reconnection may explain this regional local time control of discrete aurora on Mars.

Introduction

Auroral emissions are bright features in a planet's atmosphere caused by collisions between atmospheric particles and precipitating electron populations. Precipitating electrons collide with the atmosphere and accelerate along open magnetic field lines, producing auroral emissions. On Earth, these emissions occur in the visible range of the spectrum forming the Aurora Borealis; on Mars however, these emissions appear as bright carbon monoxide emissions in the mid-ultraviolet range, from ~185 to ~325nm.

There are three types of known aurora on Mars – discrete, diffuse, and proton aurora. Discrete aurora are patchy and sporadic ultraviolet (UV) emissions localized in time and geographic location on Mars (Bertaux et. al. 2005). These emissions are caused by collisions between atmospheric particles and precipitation electron populations and are highly correlated to martian crustal magnetic field. Diffuse aurorae cover the martian nightside and is attributed to ~ 100 keV solar energetic particles (Schneider et al., 2015.) Penetrating solar wind protons cause proton aurora and occur mostly on the martian dayside (Deighan et al., 2018.)

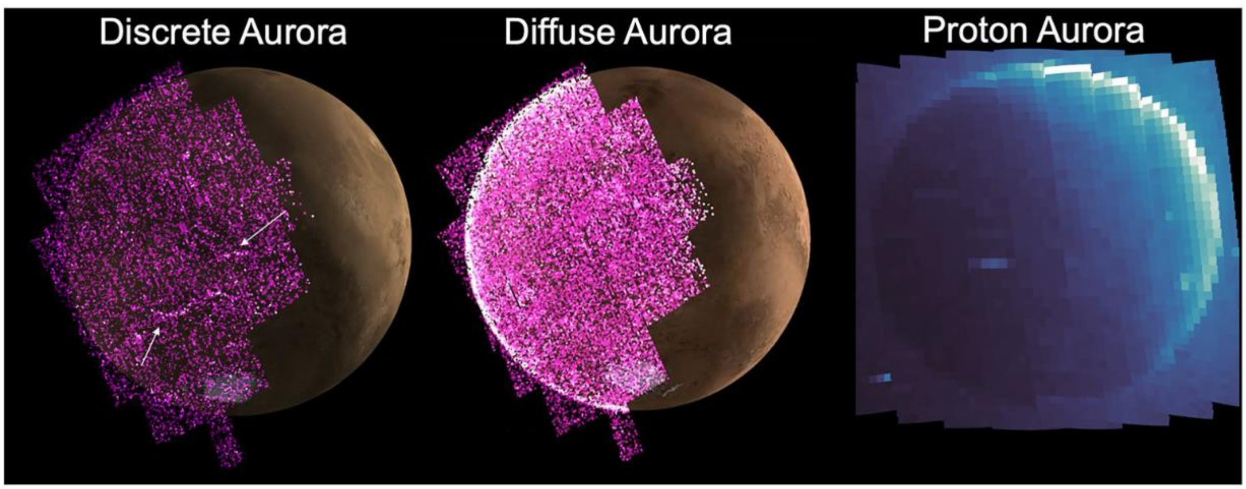

Figure 1. MAVEN IUVS apoapse images showing three distinct types of aurorae from orbits 5738, 5831, and 849. *Figure Credit: Schneider 2021*

Discrete aurora on Mars was first identified by the ultraviolet spectrograph (SPICAM) on Mars Express (Bertaux et. al. 2005) which appeared as clustered, sporadic, and localized emissions in the mid-ultraviolet. Further work conducted by the SPICAM team (Leblanc et al., 2006, Leblanc et al., 2008, Gerard et al., 2015) expanded the list of detections to 19, 16 of which were identified in nadir-viewing geometry. This work showed that (1) the lifetime of discrete aurora is on the second timescale and (2) correlations between detection time and electron energy measurements (taken by the ASPERA-3 instrument aboard the Mars Express) showed that detection locations were highly correlated with locations of increased precipitating electron fluxes (Gerard et al., 2015.) These SPICAM detections were plotted on top of a global crustal field map (Brain et al., 2007) and found to be correlated with local field strengths. Analysis of precipitating electron populations with contemporaneous SPICAM aurora detection times (Brain et al., 2006, Gérard et al., 2015, Leblanc et al., 2006, Leblanc et al., 2008) with models of electron energy deposition and resultant emission altitudes (Leblanc et al., 2006, Soret et al., 2016) revealed the emission populations causing discrete aurora and altitude. These electron populations are likely between 40-200 eV and peak near 130 km altitude (Brain et al., 2006, Soret et. al. 2021.)

Later work, conducted 10 years later using MAVEN-IUVS observations, revealed the first nadir-viewing full-disk image of discrete aurora on Mars. In this work, the IUVS team identified a single orbit during the September 2017 space weather event with multiple discrete aurora emissions (Schneider et al. 2018.) Due to the lack of a large nadir-viewing dataset of detections, it remained unanswered at the time if discrete aurora were visible in other nadir-viewing observations.

Analysis of MAVEN-IUVS limb observations confirms previously reported knowledge of crustal field strength correlations with both detection location and brightness and auroral emission altitude (Schneider et. al., 2018, 2021.) This analysis also showed events mainly occurring before midnight with a preference for negative interplanetary magnetic field (IMF) clock angles in the strong crustal field region (Schneider et al., 2021.) Due to observational bias and spacecraft viewing limitations, this dataset did not have good morning coverage. It remained unanswered how local time controlled where discrete aurora occurred.

The work presented here builds off previous understanding and examines an additional seven thousand nadir-viewing observations of Mars using MAVEN-IUVS data. This independent and in-depth analysis has resulted in an additional 183 detections, confirms previous understanding of discrete aurora, allows for tighter confinement on detection locations and dimensions, and reveals a previously unreported regional local time correlation of discrete aurora on Mars.

Methods

MAVEN is a spacecraft orbiting Mars with nine instruments on board each with a specific role (Jakosky et al., 2015). Three examples of the instruments onboard MAVEN are the Imaging UltraViolet Spectrograph (IUVS), the Solar Energetic Particle (SEP) instrument, and the Neutral Gas and Ion Mass Spectrometer (NGIMS). The analysis presented in this paper uses data obtained by the IUVS remote-sensing instrument. The IUVS slit is narrow and spans ~ 11^{o}x0.06^{o} giving it a well-defined instantaneous field of view. By using a rotating scan mirror on an articulating platform, IUVS has two fields of regard (FOR), limb and apoapse. The scan mirror switches between these two FORs depending on where MAVEN is in its orbit. The limb and apoapse FOR spans approximately 24^{o}x12.5^{o} and 60^{o}x12.5^{o}, respectively ((McClintock et al., 2015).) The IUVS instrument (figure 2) records spatial-spectral images in two regions of the spectrum, mid-ultraviolet (MUV) and far-ultraviolet (FUV). For this work, I have analyzed data taken using mid-ultraviolet detector in the apoapse observing mode.

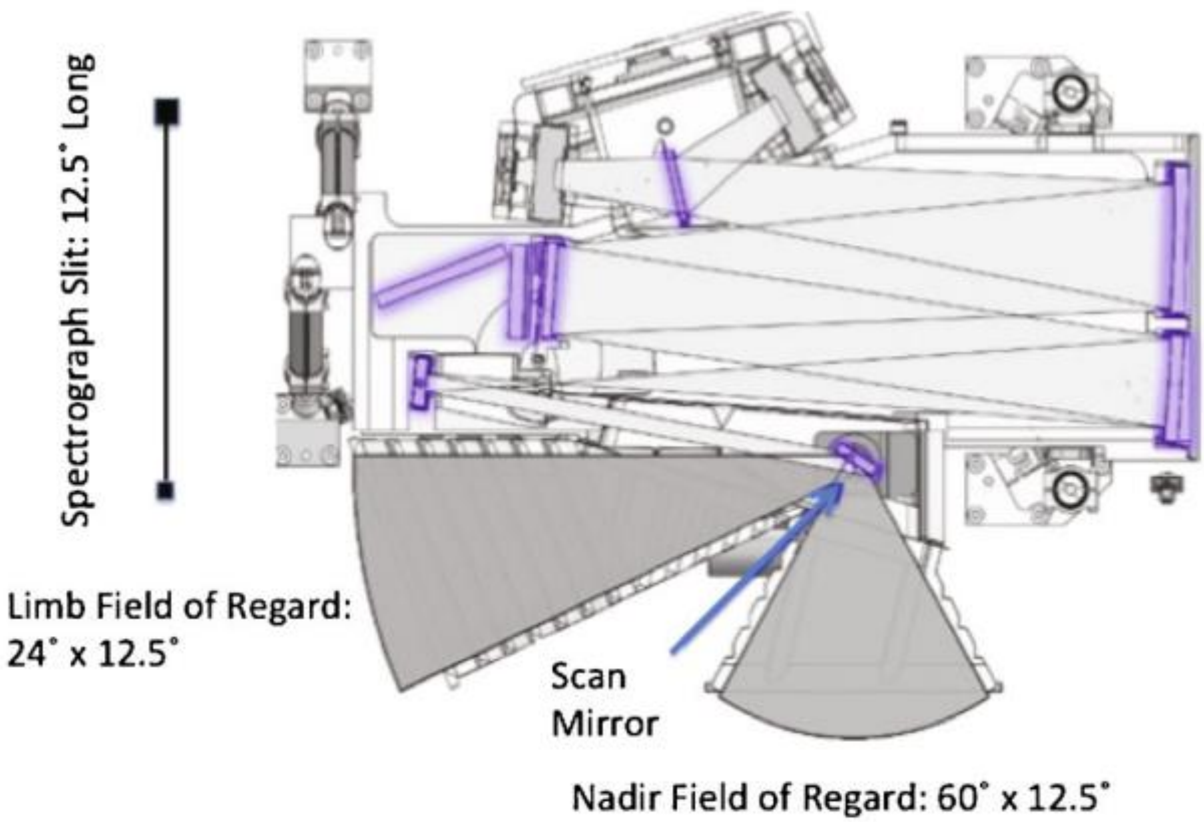

Figure 2. CAD drawing showing the IUVS instrument (McClintock et. al., 2015)

MAVEN’s unique orbit around Mars allows for two different observation modes of discrete aurora on Mars, each with their own advantages and disadvantages. Figure 3 shows the orbit of the MAVEN spacecraft around Mars. MAVEN’s orbit is highly eccentric, with a periapse altitude of ~380 km and an apoapse altitude near ~6250 km. The low periapse allows IUVS to take accurate atmospheric measurements to understand atmospheric composition and structure, while a high apoapse allows IUVS to record full disk images through the combination of spacecraft motion, planetary rotation, and spectrograph slit scanning. At apoapse, the IUVS instrument is looking within tens of degrees of perpendicular to the disk (nadir observations), while at periapse (limb observations) the instrument observes tangent through the atmosphere and scans vertically to build altitude profiles.

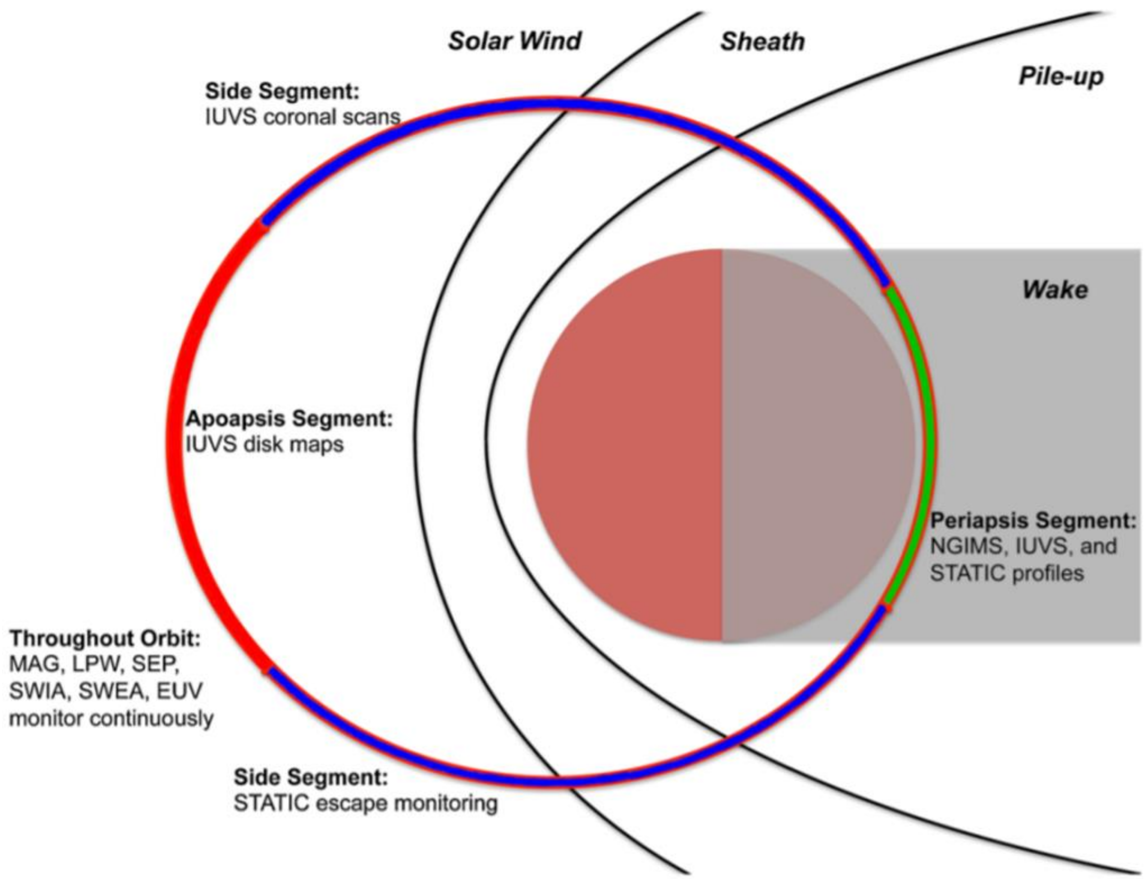

Figure 3. MAVEN orbit around Mars with observation segments labeled. The sun is to the left of Mars. Figure credit: Jakosky et al., 2015.

Discrete aurorae events are identifiable by their spatial and spectral characteristics. Auroral signatures appear in apoapse orbits as snake-like features, bright in color, corresponding to CO Cameron Band emissions. Discrete aurorae are comprised of carbon monoxide (CO) emissions and thus these discrete aurora detections are characterized by the intensity of CO emissions in each pixel on the nightside of the martian disk. These features appear sporadically across the globe as either long strings covering multiple pixels and hundreds of kilometers long on the disk, or as small blotches covering only tens of kilometers of the disk. Figure 4 shows three example apoapse images, each with various real and non-real discrete aurora emissions. For each detection, multiple pixels make up a single detection; the process by which I chose these pixels is outlined in following paragraphs.

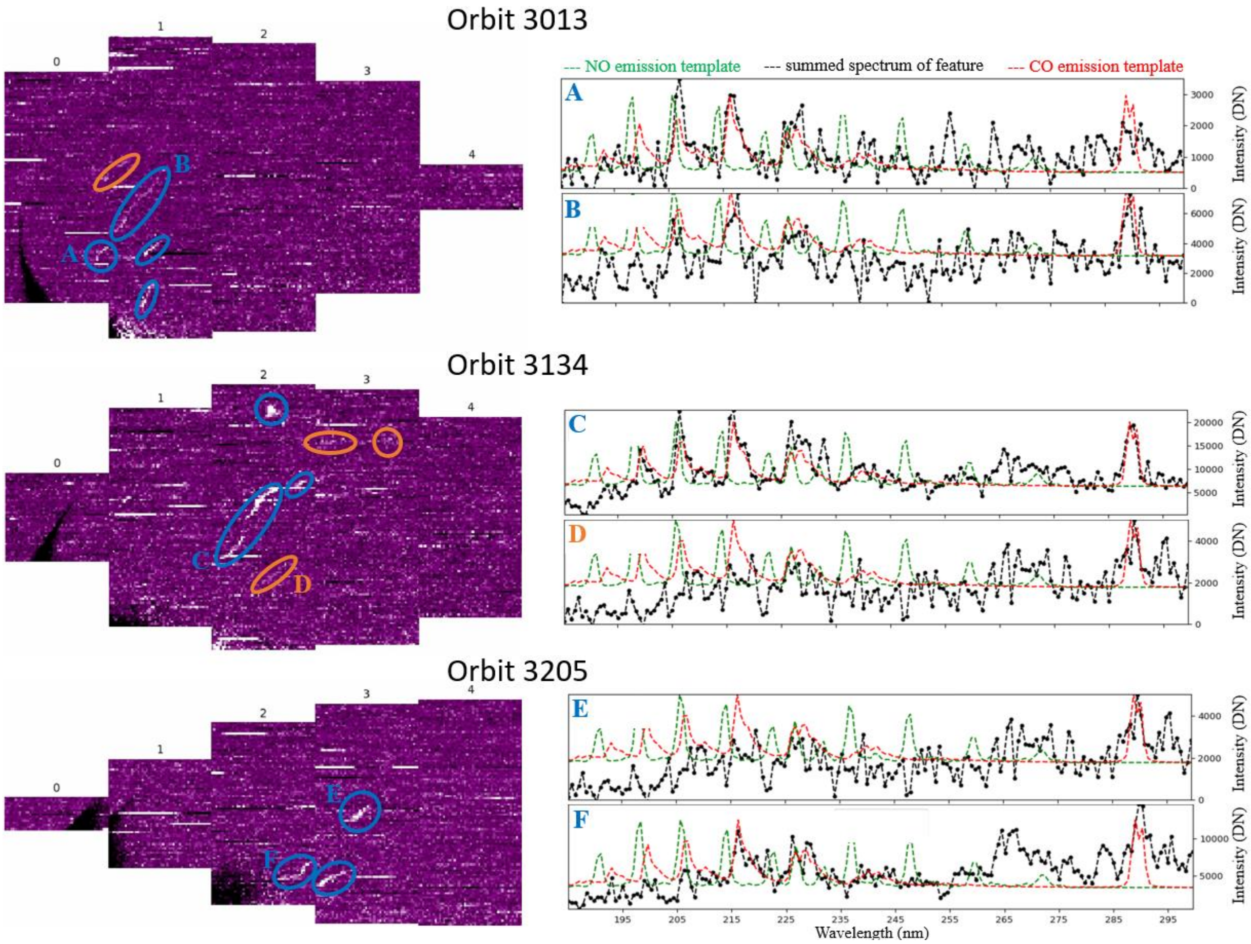

Figure 4. Three example nightside apoapse disk images (left) with real and non-real discrete aurora spectra for several features (right) The purple-white colorbar corresponds to CO emission intensity, ranging from 0 - 1.5+ kR (black - white). The blue circles on the images locate real discrete aurora detections, while orange circles locate non-real ones caused by detector artifacts, cosmic rays, or solar continuum leaking into the CO fit. The spectra of five real and one non-real detections are shown in the right column, with labels corresponding to the circles on the images.

MAVEN's 14500 orbits around Mars have yielded 6933 apoapse images. To analyze all available nightside apoapse data for signatures of discrete aurora, I generated movies in hundred orbit blocks for all available orbits. Each frame of these movies is an apoapse image from a specific orbit, which I visually analyzed for auroral signatures. Examples of such signatures are shown in labeled circles A-F in figure 4. I recorded any orbit showing visual signs of aurora and later analyzed them with a spectral query tool to determine if the suspected emission was real.

Due to the global view in apoapse observing, multiple pixels make up a single feature as each pixel cover ~45x60km on the martian surface. Special L2B images were produced for my analysis for all available orbits with apoapse observations. The L2B apoapse images 4-dimensional arrays, two dimensions for the spatial component (i.e., a 2-D disk image), one for the spectral component of each pixel, and the fourth for the indexing specific pixels. On average, there are ~ 25,000 pixels per apoapse image. Each pixel contains: (1) a spectrum ranging from ~185-325nm, reported in data number (DN)/nm, (2) a MLR fit value representing the amount of CO emission in said pixel, and (3) geometric and observational information including latitude, longitude, local time, emission angle, and solar zenith angle. MLR stands for "multiple linear regression," which fits a CO emission template to the data to determine the intensity of CO in said pixel. This fit value is obtained through the pipeline production process for L2B images. These L2B files also contain MLR fit values for CO_2^+ (CO ultraviolet doublet, UVD), nitric oxide (NO), and solar continuum (SS) emissions for each pixel, along with spacecraft geometry (i.e., spacecraft altitude, emission angle), pixel geometry (i.e., latitude, longitude, solar zenith angle, local time), observation information, and instrument information.

To analyze each recorded orbit, I needed a tool which utilized spectroscopy to determine the validity of each visually identified discrete aurora detection. I created this tool from scratch and used it to analyze each pixel of individual features from suspected orbits for signatures of CO emissions. Multiple pixels, each with their own unique spectrum, make up a single feature. Figure 5 shows an example of this spectral query tool in use. The tool allows the user to look at the spectrum of an individual pixel compared to a template aurora spectrum, sum the individual spectrum from each pixel in a feature into a single spectrum, and compare the summed spectrum with a template to determine if the suspected auroral spectrum was real. The summed spectrum was then correlated to a template spectrum for CO emissions using a Pearson-r correlation. A detection was real if the Pearson-r correlation was greater than 0.5, as this indicates the features' peaks are highly correlated with those of CO emissions. This threshold was set through analysis and follows a similar threshold based on the detection algorithms from previous limb detections

(Schneider et al., 2020). I did not use any magnetic field or geographic information to determine if a detection was real or non-real.

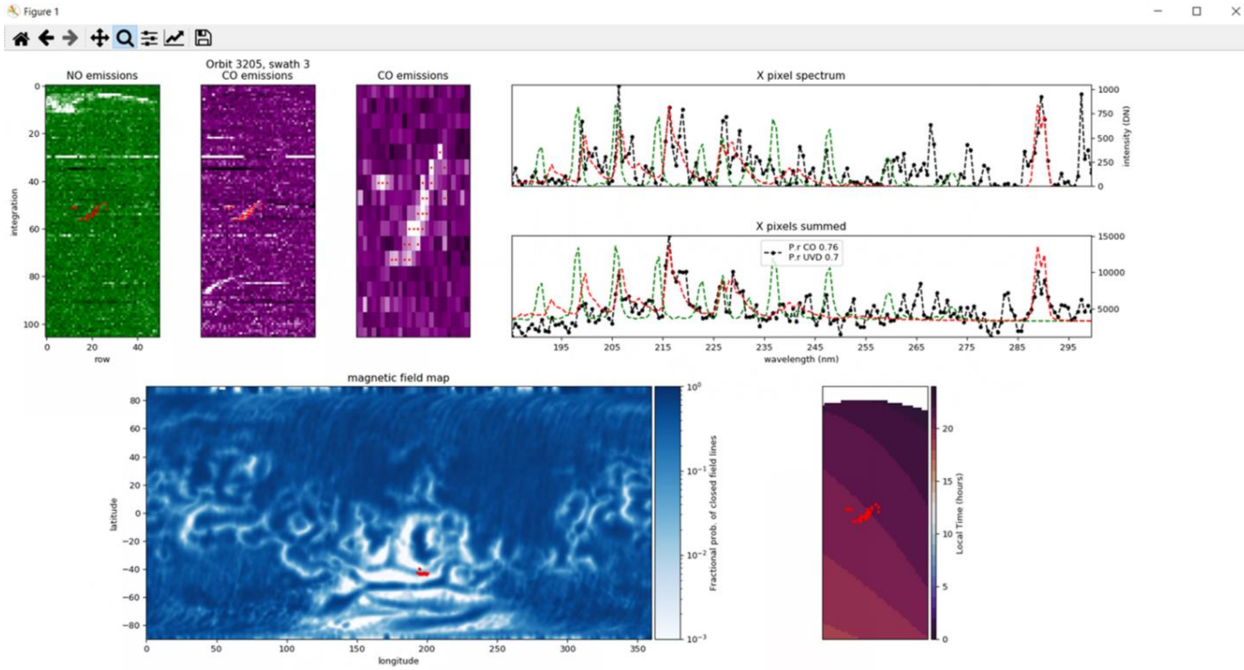

Figure 5. Example of interactive spectral query tool. This tool allows the user to load an apoapse image, zoom in, and analyze the spectra of each pixel in a feature, co-add all the spectra in said feature, and save a file containing all relevant information about the feature, including geographic, local time, emission angle, and spectral information for each pixel for later analysis. The purple-white colorbar shows CO emission intensity from 0 to 1.5+ kR.

In this analysis, I implemented several measures to determine if an individual pixel in a feature showed real auroral signatures. First, only pixels with CO intensities at least 1.5x the background intensity were included in the list of pixels making up a single feature. Second, I only included pixels with a “clean” spectrum. A “clean” spectrum does not contain spectral spikes, solar continuum contamination, or cosmic ray artifacts.   If a pixel in a suspected auroral feature had a spectral spike (~5x increase in signal compared to background noise, at a single wavelength), contained solar continuum (~10x increase in signal compared to background noise, above 200nm), or contained cosmic ray noise (broadband increase in signal, across spectrum), the pixel was not include in the list of pixels for said feature. I used the spectral tool (figure 5) to manually select and analyze each pixel in a detected feature to ensure all included pixels were real and did not contain significant artifacts.

After analyzing every apoapse image *(.fits* format*)* for visual signs of discrete aurora and making a list of suspected orbits with emissions, I went through said list of suspected emissions and using the spectral query tool for each, manually located the pixels for each suspected detection, and finally determined if the detection was real based on a Pearson-r correlation. If the detection was real, I would save a data file *(.npy* format*)* for that specific detection using functions I built into the tool. Examples of included data in these files are filename, orbit number, and pixel data for the selected pixels making up a detection feature, including local time, latitude, longitude, spacecraft altitude, and pixel emission angle. The *(.npy)* detection files contain multiple arrays for each quantity described above for ease of indexing and analyzing all detection parameters together. After I confirmed which detections were real detections and recorded the *(.npy)* detection file for each, I plotted the geographic locations on a global magnetic field map of Mars to understand where emissions were occurring.

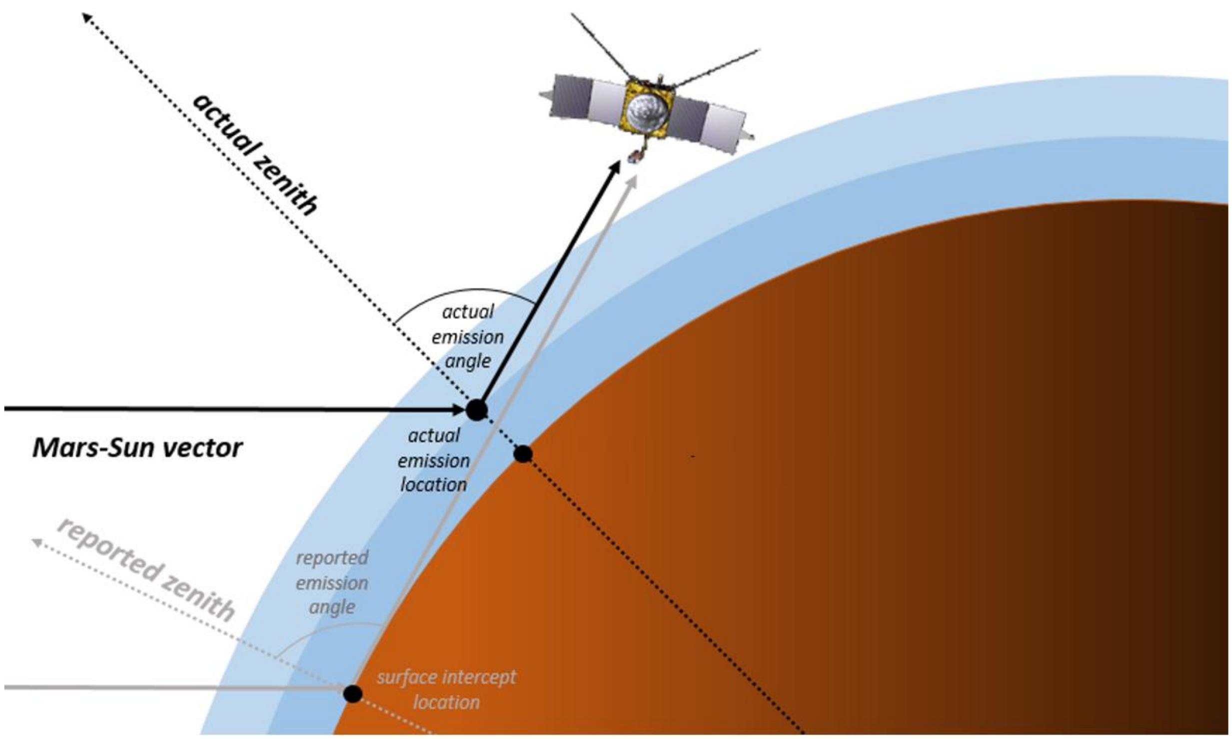

Figure 6. Cartoon showing line of sight ambiguity caused by large spacecraft emission angle. The angle between the spacecraft line of sight and vector normal to the disk at the spacecraft's location can be large when IUVS is looking at the edge of the disk. This happens for most apoapse observations when IUVS is observing near the edges of the disk, resulting in incorrect reported latitude/longitude and local time values for detected auroral pixels.

Plotting each detection location on the global magnetic field map of Mars revealed detections in locations we did not expect based on physical principles (i.e., particles should not precipitate on closed field lines.) This was due to a lack of correction in emission angle and emission altitude in the reported location of pixel geometry. While nadir observations have nearly orthogonal viewing of the disk, there are instances near the edges of the disk where the emission angle between the spacecraft line of sight and relative normal to the disk become quite large. Any detection identified in these regions requires a substantial correction due to the spacecraft emission angle relative to surface normal. IUVS records a specific latitude and longitude value for each pixel interpolated based on the spacecraft's line-of-sight, and do not account for the two things. First, the angle between the spacecraft line of sight and normal to the disk are not accounted for (emission angle.) Second, reported pixel locations do not account for auroral emission altitude. All latitudes and longitudes reported in apoapse image files assume the emissions occur at 0 km on the martian surface. This is not the case, however, because previous work has shown that aurora occurs ~130km above the surface. Thus, each correction needed to be mapped onto a sphere surrounding Mars at 130km altitude above the martian surface. Figure 6 shows a cartoon of how spacecraft emission angle and auroral emission altitude can affect geographic detection location.

I corrected the location of each pixel in all real detections for both spacecraft emission angle and auroral emission altitude using SPICE kernels. SPICE kernels store information about which planetary body a spacecraft is orbiting, relevant coordinate systems, and useful geometric calculations and corrections for specific parameters, including projecting locations along a line of sight. The correction for emission angle and emission altitude shift detection locations to regions of higher probabilities of open field lines and stronger crustal fields (figure 7.) I used the corrected dataset for the remainder of my analysis.

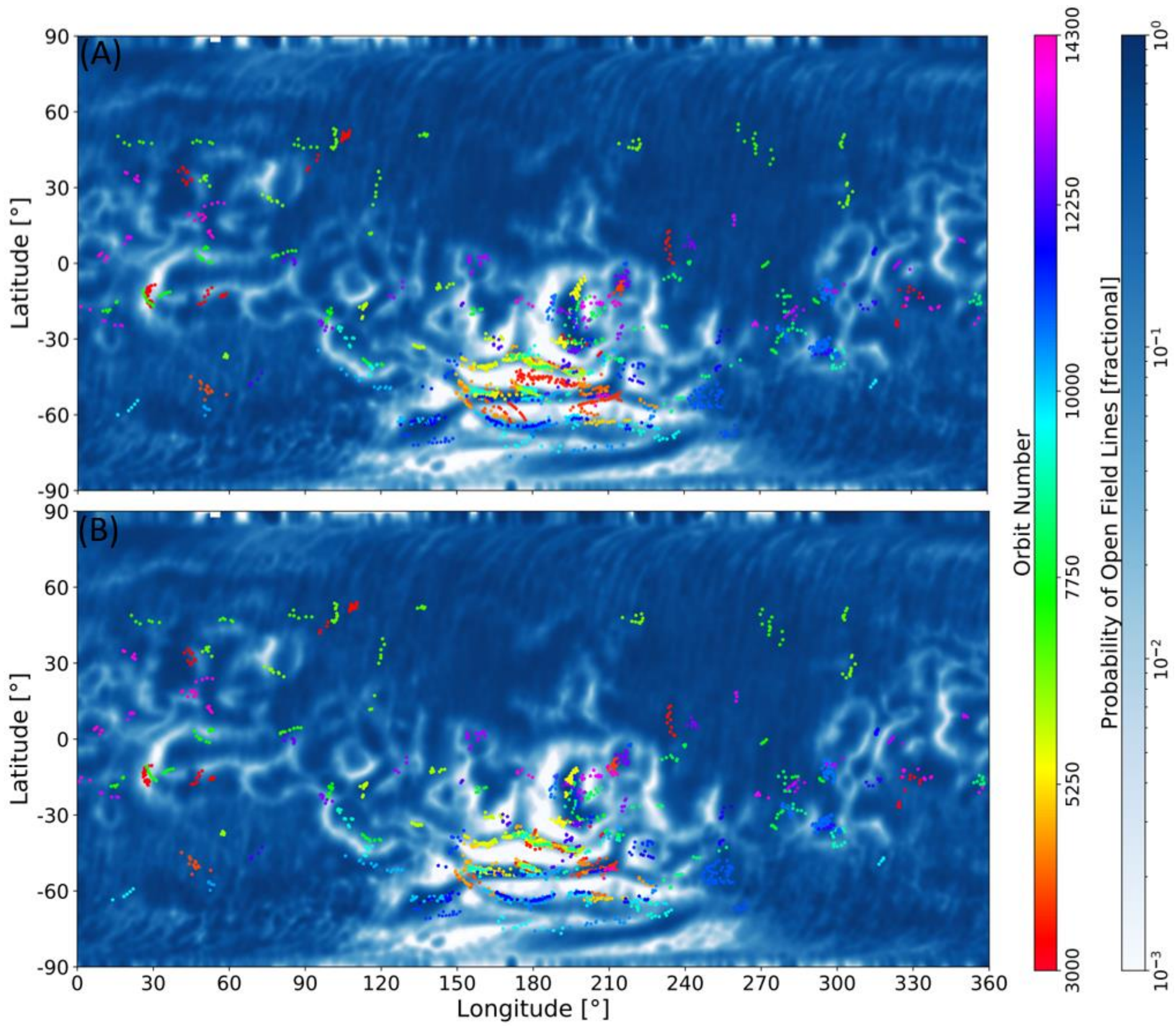

Figure 7. The top plot shows the locations of all detections prior to the emission angle and auroral emission altitude correction, while the bottom shows locations post-correction.

Results

Discrete aurora are very sporadic events and require proper viewing geometry to observe. Discrete aurorae are much more likely to occur in the strong field region, and observations covering this region make up ~14% of all apoapse observations. Of this 14%, only ~6% of these observations show discrete emissions. Between orbits 3000 and 14300, 6933 orbits contained nightside data. 5896 of these orbits had good nightside coverage, where more than 30% of the nightside was visible in apoapse images. IUVS observed the strong crustal field region 1276 times in the apoapse observing mode with good disk coverage. Overall, 183 individual detections from 119 orbits contained discrete aurora from these 5896 orbits, and 76 detections from 38 individual orbits occurred in the strong crustal field region.

Discrete aurora can occur globally and sporadically, however detections in the strong field region make up ~43% of all detections and are ~ 20 times more likely to occur near strong fields. Figure 8 shows detections in the strong field region. Emissions identified in the strong field region show high repeatability and repeatedly fall along the same open field line contours. This repeatability is visible in figure 8 by the overlay of detections in nearly the same locations. Detections near -50° latitude and 175° longitude, which appear diagonal and overlay tightly with each other (figure 7), fall directly on top of the highest strength crustal field (>762 nT). In this plot, each detection is color coded by orbit. Since a single detection can contain multiple pixels, each with a specific latitude/longitude, all pixel locations of a detection are plotted on this map. This helps to show the spatial extend and string-like nature of emissions.

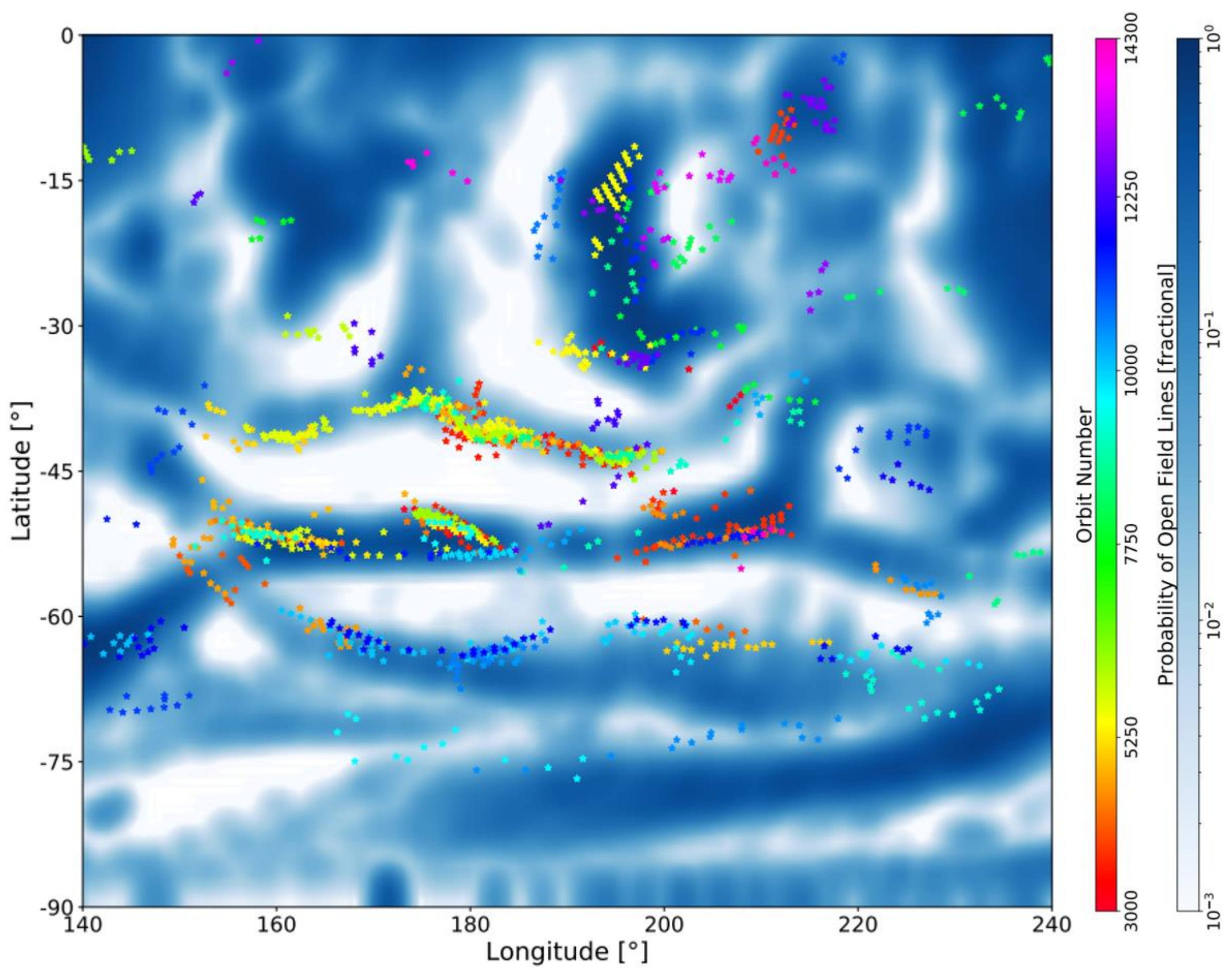

Figure 8. Discrete aurora detections overplotted on open field line probability map showing only the strong crustal field region. The rainbow colorbar corresponds to orbit number.

Aurora are ~20 times more likely to occur in the strongest crustal field locations of Mars and align very well with "valleys" of high-probability open field line regions. This agrees with previous results found in limb observation analysis where aurora occurred ~40 times more frequently in strong fields (Schneider et al., 2021). Figure 9 shows the correlation between aurora detection frequency and crustal field strength. A crustal field map using sub 250km MAVEN observations (Weber et al., 2020) was used to assign a radial crustal field value to each nadir auroral detection and non-detection. An "observation" in this scenario is defined at the pixel-level, because each detection "feature" consists of several pixels, and each pixel corresponds to a different crustal field strength. I calculated detection frequency by dividing the number of detections by the total observations in each bin to remove observation bias . Next, I binned the results logarithmically to better show small variations in detection frequency between each decade change in magnetic field strength. IUVS observed field strengths >562 nT (rightmost bin) in ~350 orbits over the ~7000 orbits analyzed, and 13 of these orbits contained discrete aurora.

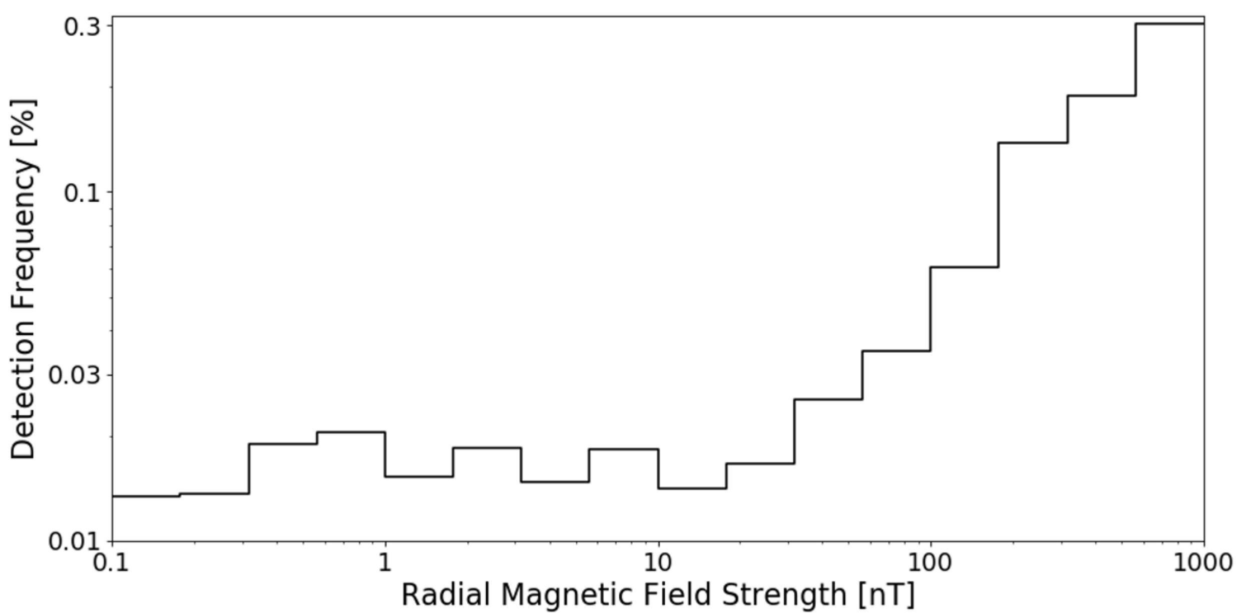

Figure 9. Detection frequency vs magnetic field strength. Magnetic field values are binned logarithmically using four bins per decade. The black line shows the distribution after the emission angle and altitude correction was applied.

This dataset shows previously unreported correlations between regional and local time control of discrete aurora in the strong field region. To understand variations in the local time control, I defined two adjacent regions and analyzed the local time distributions for in each.

Figure 10 shows detections color coded by orbit number in the northern and southern regions with corresponding local time detection frequency histograms for each region. The northern "arcade" (gray box) extends from -35° to -52° latitude, and the southern arcade from -52° to -69° latitude (red box.) Both regions span 150° – 210° longitude. Local times are binned in 1-hour increments from 6pm local time to 7am local time, centered at midnight. In the northern region, there are 51 detections from 31 orbits and 37 detections from 16 orbits in the southern region. In the northern region, most detections occur pre-midnight near the dusk terminator, and in the southern region, the majority occur post-midnight, mostly near the dawn terminator. The error bars are derived from counting statistics, where the error on the number of detections in each local time bin is given by $\frac{\sqrt{(\#Detections\ in\ a\ bin)}}{\#Observations\ in\ bin}$. For these arcade maps, I split the dataset was into two groups: northern and southern. All pixels IUVS observed within the northern region were counted as observations in said region, and the converse is true for the southern region.

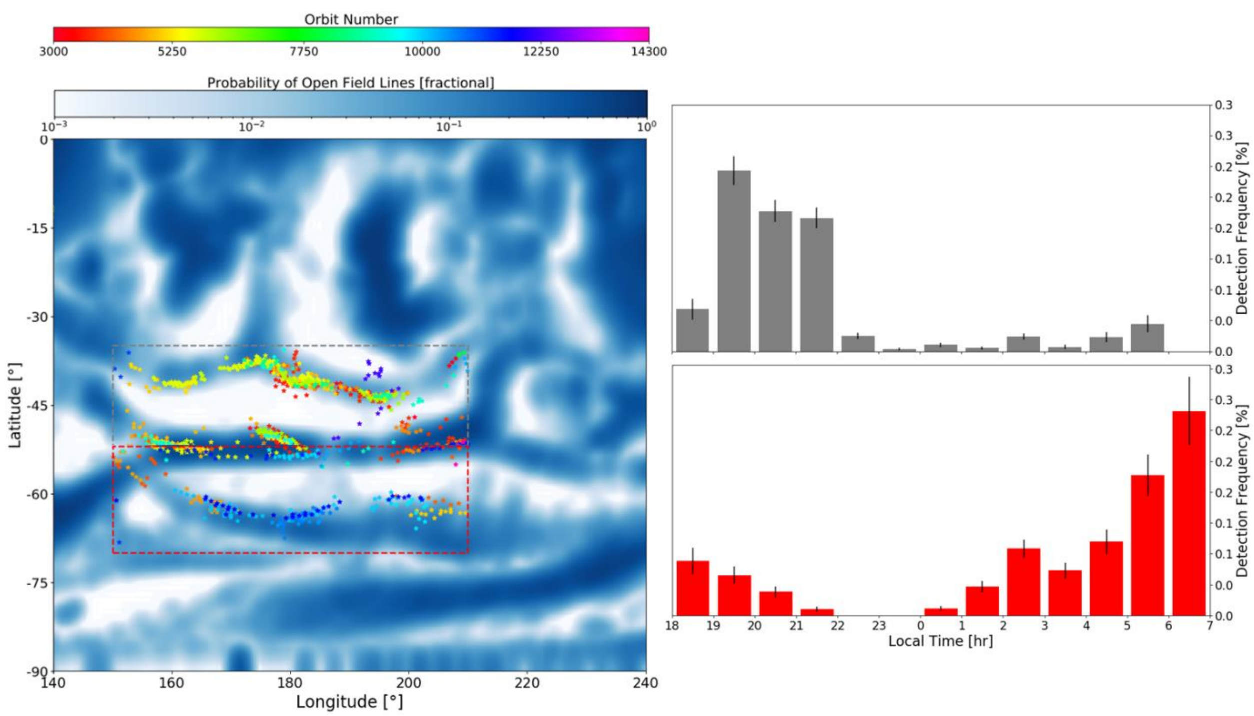

Figure 10. Open field line map with northern and southern region boxes drawn and detections in each region overplotted using the rainbow colorbar corresponding to orbit number *(left)*. The local time detection frequency histograms for the northern (gray) and southern (red) regions are shown with included error bars. The local times are centered around midnight and binned in military time, with hour 18 corresponding to 6am local time (dusk terminator), 0 being midnight, and 7 being 7am local time (morning terminator).

The intriguing local time flip between the two adjacent regions shown in figure 10 led me to plot the detections on a global magnetic field map in a more unique and simpler format. Instead of using a rainbow colormap corresponding to orbit number, I plotted all detections on the same martian field map using a bimodal red/black colormap corresponding to pre-or-post midnight detection local time. Detections occurring before midnight (dusk terminator) are shown in red while detections with post-midnight (dawn terminator) local times are shown in black. Plotting the detections in this way revealed a noticeably clear distinction between pre-and-post midnight at -52° latitude and between 150° – 210° longitude. Analysis of detection frequency vs local time histograms shows that most pre-midnight detections from -35° to -52° latitude occur shortly after dusk. Post-midnight detections from -52° to -67° latitude mainly occur before dawn (see figure 11.)

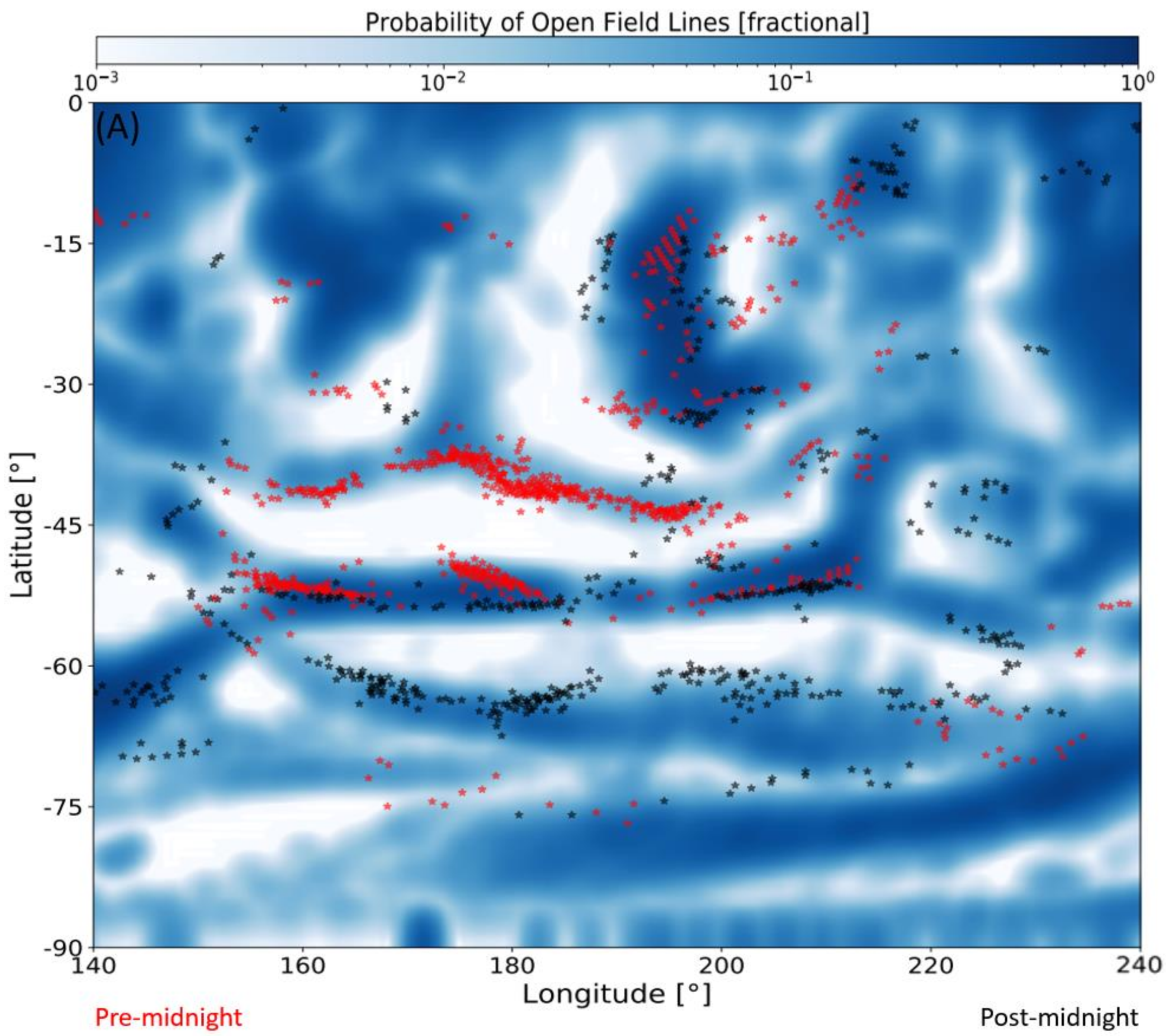

Figure 11. Detections in the strong crustal field region organized by local time. Red dots correspond to pre-midnight detection locations and black to post-midnight detection locations.

Discussion and Conclusions

Analysis of 7000 apoapse images taken by the IUVS instrument has resulted in 183 additional discrete aurora detections from a previously unstudied dataset, 78 of which (~43%) occurred in the strong field region of Mars). Before analyzing the local time control of discrete aurora on Mars using the new nadir-viewing dataset, I verified previous work performed by Schneider et al. 2021 using the detections identified in this new and independent dataset. These 183 nadir detections occurred globally, with the seventy-eight detections in the strong crustal field region showing strong correlations with local radial field strength and preference for negative interplanetary magnetic field values, confirming results found by Schneider et al., 2021.

This new nadir dataset allows the geographic dimensions of detections to be constrained due to the global view of the martian disk provided by this observing mode. Data pixels in apoapse observations have physical dimensions of ~45 x 60 km length. Detected auroral features, spanning multiple adjacent pixels, range from 1-3 pixels in width and 2-25 km in length, corresponding to physical detections dimensions between ~45 – 135 km wide and ~120 – 1500 km long. A global magnetic field map of Mars with overplotted detection locations shows the "string-bean"-like extent of these emissions (figure 5B.) Previous work using limb data did not allow such confinement because of line of-sight ambiguity and limited disk coverage.

The regional local time behavior of detections identified in the strong field region give insights to the existence of two adjacent crustal magnetic field "arcades" with opposite horizontal fields. Figure 10 shows a cartoon showing two "arcades" that form in the strong crustal field region, resulting in three "bands" of detections. In figure 10, auroral detections occur along the black dashed lines, where crustal magnetic fields either originate or terminate on the surface (open field lines.) Discrete aurorae identified in the southern loop occur when the post-midnight sector is near the dawn terminator, while detections along the northern loop occur primarily near the dusk terminator when the northern loop is in the pre-midnight sector. The emissions in these regions show preference for $-B_{Y,MSO}$ IMF orientation, consistent with the results from Schneider et al., 2021 and Girazian et al., 2022.

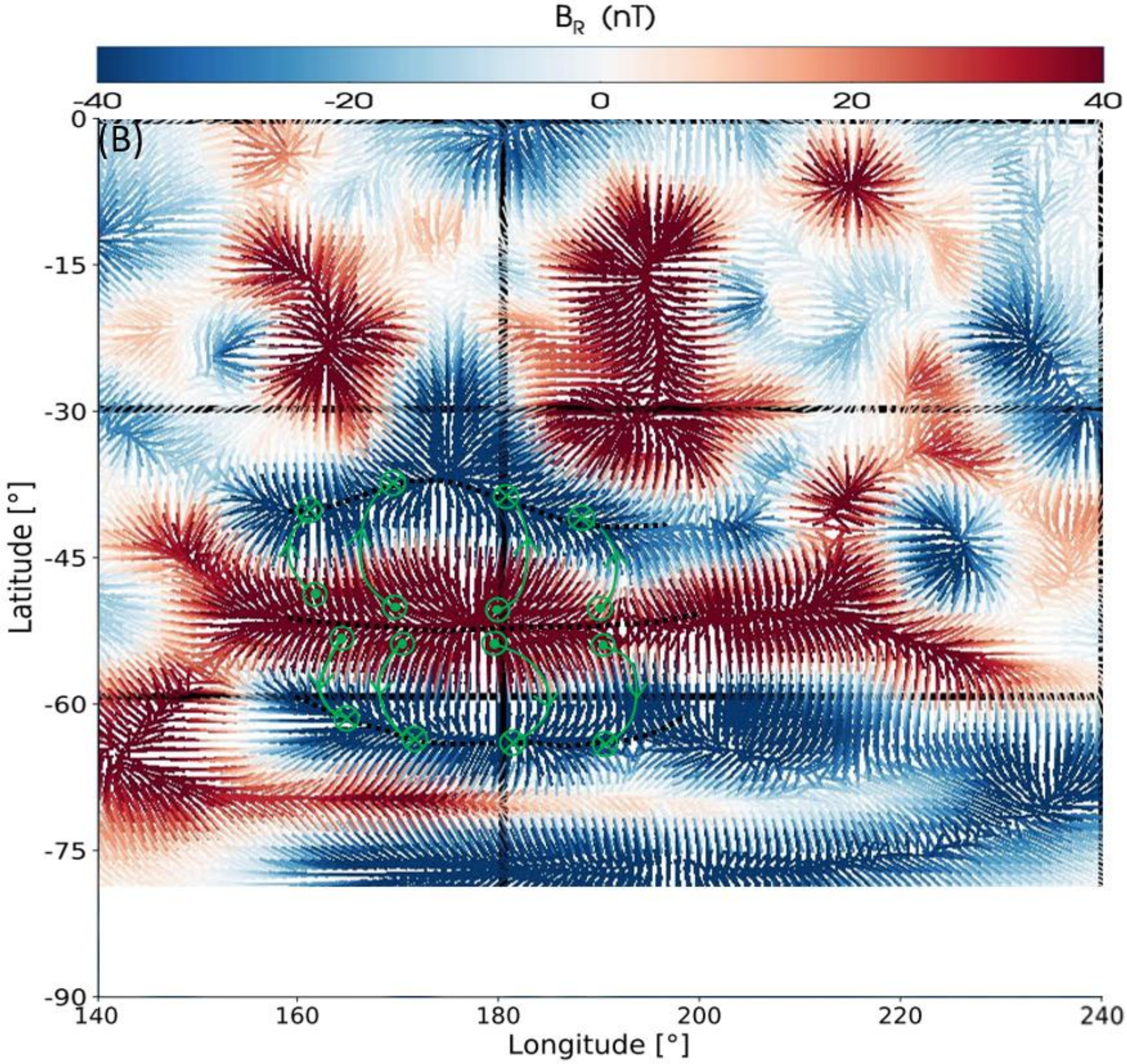

Figure 10. "Whisker" magnetic field plot of the strong field region. This plot has arrows showing local crustal field orientation below 250km, and color showing direction and strength. Blue lines have negative strengths corresponding to field lines ending in these locations, while red lines show where field lines originate. The top black dotted line near -35° latitude is the "boat deck", the dotted line near -52° latitude is the "waterline", and the final line near -70° latitude corresponds to "below the wave". The green lines show a 3-D representation of crustal field lines originating from the "waterline" and closing on either the "boat deck" *(northern arcade)* or "below the wave" *(southern arcade),* both in agreement with local crustal field direction and orientation. *Figure Credit: David Brain*

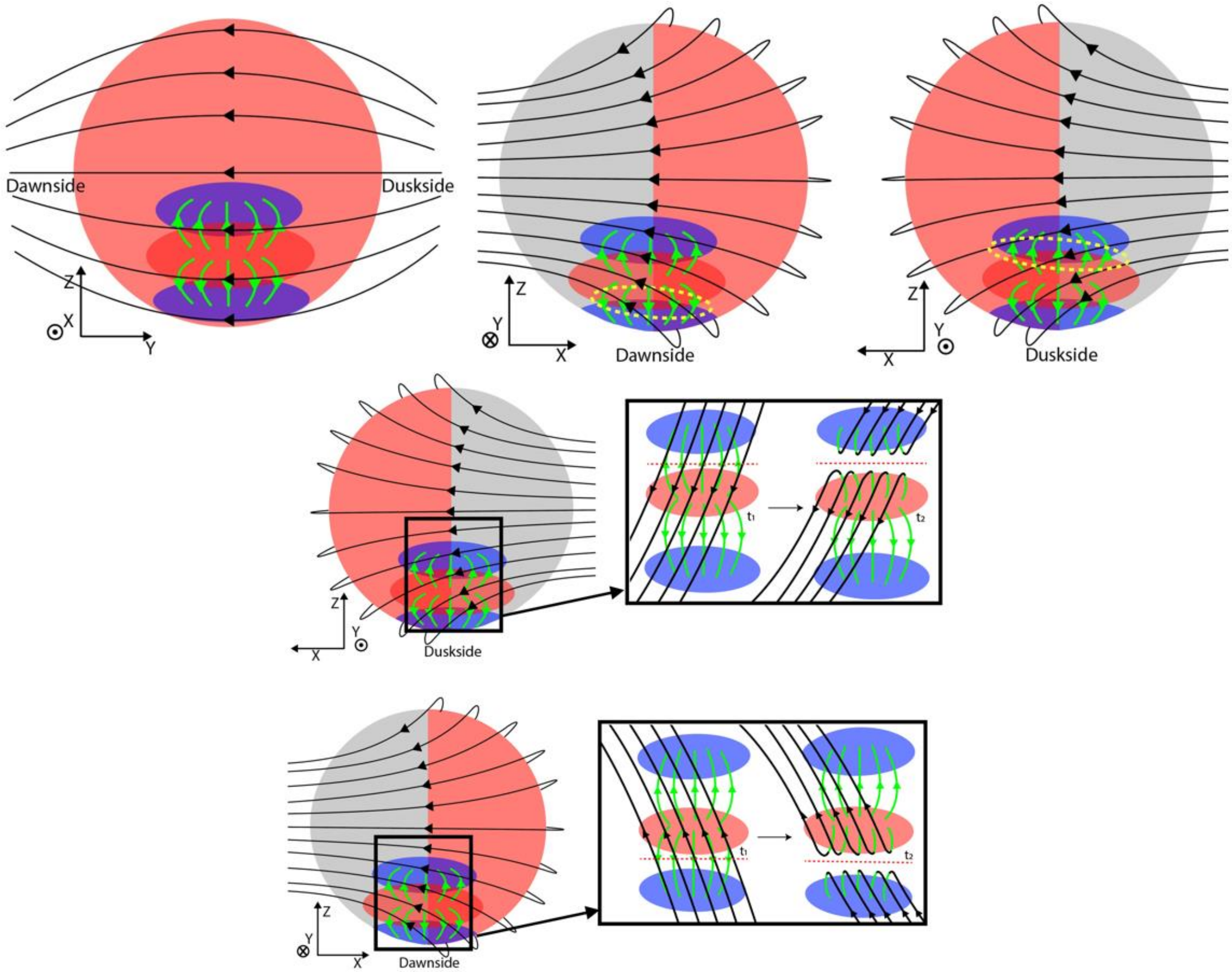

Figure 11. This figure shows the draped interplanetary magnetic field for a -By field line (black arrows). The top three cartoons show the orientation of the strong crustal field region at midnight (left), dawn (middle), and dusk (right). The middle cartoons show the duskside orientation and reconnection preference for the northern arcade, and the bottom illustration shows the dawnside equivalent, where geometry between the crustal fields and the draped IMF favors reconnection for the southern arcade. *(Figure credit: Charlie Bowers)*

Discrete aurorae occur where reconnection opens closed local magnetic field loops and creates magnetic "valleys" for charger particles to accelerate and precipitate into the atmosphere, producing emissions at 130km altitude. Reconnection is much more likely when a large shear angle between the local crustal loops and the imposed field exists. In this case, this is the relative angle between the north/south component of the local crustal fields and the north/south component of the draped interplanetary magnetic field. A representation of this is shown in figure 11, which demonstrates how a draped magnetic field configuration (Fang et al., 2018) would appear from the dayside, dawnside, and duskside of the planet. On the dayside of the planet, the draped IMF is at a low shear (~90°) to the crustal field region and is therefore unlikely to undergo reconnection. On the dawnside of the planet (Figure 4b), the draped IMF has been shifted northward and is therefore more susceptible to reconnecting with the crustal magnetic field lines closing southward due to the large shear created between these fields. This suggests that on the dawnside (post-midnight), discrete auroral emissions are more likely to be detected over the footprints of the southern crustal magnetic field loop. The opposite is true for the duskside (Figure 4c), in which a southward shifted draped IMF creates a large shear with the northern crustal loop, making it more likely for reconnection to occur in this region and, therefore, more likely for the activation of auroral emissions.

In summary, an independent and comprehensive analysis of all IUVS nightside apoapse data revealed 183 additional discrete aurora detections, confirmed previous understanding of discrete aurora found in limb observation analysis, and reveals local time control for emissions occurring in the strongest crustal fields. Magnetic reconnection between local martian crustal fields and the draped interplanetary magnetic field may explain the observed control between detection local time and regional occurrence, however further work is required to determine how seasonal variation and martian tilt will affect magnetic field reconnection geometry.

Future Work

While this work expands the nadir viewing dataset detection list, confirms previous understanding, offers insights into emission locations and dimensions, and answers questions regarding local time and regional control of discrete aurora, there remains unanalyzed data and unanswered about discrete aurora on Mars. For instance, there are several regions inside the strong crustal field region void of detections in both limb and nadir datasets. I have ruled out observational bias for this by comparing spacecraft geometry and various detections at limb and apoapse observational modes, so it remains unanswered why these regions do not show emissions. There are ~2000 recent orbits that are unanalyzed, and several other observing modes (which cover different regions of the spectrum) to analyze for discrete aurora. In addition to analyzing observations in the mid-ultraviolet (CO emissions), observations taken in the far-ultraviolet (oxygen emissions) are also currently unanalyzed. The biggest question is how martian tilt will affect reconnection preference and if seasonal variation plays a role in determining where discrete auroral emission occur, as I have yet to analyze this for the current 183 nadir detections. Due to Mars' tilt, ~20^{o} off-axis, it is highly likely this angle will change the geometry between the local crustal fields and the draped interplanetary field. This tilt will thus change the reconnection geometry and shear angle preference between seasons on the dawn-and-dusk terminators. Two adjacent regions show local time control – further analysis and additional detections are required to determine if other regions show similar local time control. I would also like to refine my model of the "arcades" in the strong field region, for instance, instead of defining the regions using horizontal lines, creating a model with curved boundaries matching the curvature of the field line structure and topology may reveal cleaner or additional insights into reconnection. Lastly, I am currently working on an automated machine learning detection algorithm to re-analyze thousands of orbits to check for data gaps from the visual analysis method, which I have yet to finish and evaluate on the nadir observation dataset

References

Bertaux, J., et al. (2005). Discovery of an aurora on Mars, Nature, 435. Retrieved from https://www.nature.com/articles/nature03603

Brain, David., et al. (2006). On the origin of aurorae on Mars. Geophysical Research Letters. Retrieved from https://agupubs.onlinelibrary.wiley.com/doi/abs/10.1029/2005GL024782

Brain, David., et al. (2007). Electron pitch angle distributions as indicators of magnetic field topology near Mars. Journal of Geophysical Research: Space Physics. Retrieved from https://agupubs.onlinelibrary.wiley.com/doi/abs/10.1029/2007JA012435

Fang, X., et al. (2018). The Morphology of the Solar Wind Magnetic Field Draping on the Dayside of Mars and Its Variability. Geophysical Research Letters, Volume 45, Issue 8, pp. 3356-3365. DOI: 10.1002/2018GL077230. Retrieved from https://agupubs.onlinelibrary.wiley.com/doi/full/10.1002/2018GL077230

Gerard, J. C., et al. (2015). Concurrent observations of ultraviolet aurora and energetic electron precipitation with Mars Express. Journal of Geophysical Research: Space Physics. Retrieved from https://agupubs.onlinelibrary.wiley.com/doi/full/10.1002/2015JA021150

Girazian. Z., et al. (2022). Discrete Aurora at Mars: Dependence on Upstream Solar Wind Conditions. Journal of Geophysical Research, under review. Retrieved from https://www.essoar.org/doi/10.1002/essoar.10510117.1

Jakosky, B. M., et al. (2015). The Mars Atmosphere and Volatile Evolution (MAVEN) Mission. Space Sci Rev, 195 (3). Retrieved from https://doi.org/10.1007/s11214-015-0139-x

Leblanc, F. et al. (2006). Origins of the Martian aurora observed by Spectroscopy for Investigation of Characteristics of the Atmosphere of Mars (SPICAM) on board Mars Express. Retrieved from https://agupubs.onlinelibrary.wiley.com/doi/abs/10.1029/2006JA011763

Leblanc, F. et al. (2008). Observations of aurorae by SPICAM ultraviolet spectrograph on board Mars Express: Simultaneous ASPERA-3 and MARSIS measurements. Retrieved form https://agupubs.onlinelibrary.wiley.com/doi/abs/10.1029/2008JA013033

McClintock, W. E., et al. (2015). The Imaging Ultraviolet Spectrograph (IUVS) for the MAVEN Mission. Space Sci Rev, 195: 1–4. Retrieved from https://link.springer.com/article/10.1007/s11214-014-0098-7

Schneider, N. M., et al. (2015). Discovery of Diffuse Aurora on Mars. Science, 350. Retrieved from https://pdfs.semanticscholar.org/d71a/951e3571ea97ad5b587bac50892a8660ce62.pdf

Schneider, N. M., et al. (2018). Global aurora on Mars during the September 2017 Space Weather Event. European Geosciences Union, 20. Retrieved from https://meetingorganizer.copernicus.org/EGU2018/EGU2018-3546.pdf

Schneider, N. M., Milby, Z., Jain, S. K., Gérard, J.-C., Soret, L., Brain, D. A., et al. (2021). Discrete aurora on Mars: Insights into their distribution and activity from MAVEN/IUVS observations. Journal of Geophysical Research: Space Physics, 126, e2021JA029428. Retrieved from https://agupubs.onlinelibrary.wiley.com/doi/epdf/10.1029/2021JA029428

Soret, L., et al. (2021). Discrete aurora on Mars: Spectral properties, vertical pro-files, and electron energies. Journal of Geophysical Research: Space Physics, 126, e2021JA029495. Retrieved from https://agupubs.onlinelibrary.wiley.com/doi/10.1029/2021JA029495

Soret, L., et al. (2016). SPICAM Modelling and Observations of Mars Aurorae. Icarus, Volume 264, pages 398 – 406. Retrieved from https://www.sciencedirect.com/science/article/pii/S0019103515004285?via%3Dihub

Weber, T. D. (2020). The role of crustal magnetic fields in atmospheric escape from Mars (Order No. 28149912). Retrieved from https://www.proquest.com/dissertations-theses/role-crustal-magnetic-fields-atmospheric-escape/docview/2474837751/se-2?accountid=14667

Acknowledgements

I would like to thank you to my committee - Nick Schneider, Ann-Marie Madigan, Noah Finkelstein, and Dave Brain – for their advice and feedback on my thesis, as well as the years of support and encouragement during my undergraduate career.

I would also like to thank my research advisors *(N.B. Nick Schneider, Adam Kaufman)*, colleagues *(N.B. Sonal Jain, Zac Milby)*, professors *(N.B. Adam Norris, Dave Brain)*, family, and closest friends for all the assistance, support, guidance, advice, humor, inspiration, and love you have shared with me over the years. Words will never do justice your value to me.